Modeling the Spatial Response of the Airfoil Shear Probe Using Different Sized Probes

PAUL MACOUN AND ROLF LUECK

School of Earth and Ocean Sciences, University of Victoria, Victoria, British Columbia, Canada

(Manuscript received 5 April 2002, in final form 15 March 2003)

ABSTRACT

The airfoil shear probe is the only robust sensor currently available for measuring the rate of dissipation of kinetic energy in the ocean. The wavenumber (or spatial) resolution of the shear probe is determined by its physical dimensions, while the bandwidth of shear fluctuations is determined by the rate of dissipation. For most oceanic work, the conventional airfoil probe resolves the shear spectrum adequately. However, measurements taken in regions of larger dissipation rates, such as boundary layers, require a resolution beyond that of currently available shear probes. A newly designed probe, with dimensions approximately one-half of those of the conventional probe, was tested side by side with the conventional probe in a vigorously turbulent tidal channel. The relative response of the two types of probes indicates that both probes are characterized by a single-pole low-pass filter, with half-power wavenumbers of 49 and 88 cpm for the larger and smaller probes, respectively. After correction for this response, the spectra from both probes agree closely for the dissipation range 10^{-7} to 10^{-4} W kg^{-1}. Variance estimates from corrected spectra only agree with the Nasmyth empirical spectrum over a limited range in dissipation rate.

1. Introduction

The first measurements of oceanic turbulence were made using a platinum hot-wire probe designed to sense velocity and its fluctuations parallel to the direction of travel. These initial attempts to apply hot-wire anemometry to the ocean were not without complications; the wires proved to be efficient plankton catchers and were susceptible to fluctuations in temperature. The biological contamination issue was partially resolved by utilizing a metal film on a conical glass substrate (Grant et al. 1962), but signal contamination due to temperature fluctuations remained. Gargett (1978) was suspect of all hot-film velocity data taken in the thermocline by her laboratory in 1972 and 1973, due to significant temperature contamination at the high-frequency end of the velocity spectrum. Lueck and Osborn (1980) showed that the velocity signals from heated anemometers are very likely to be contaminated by environmental temperature fluctuations and this technology is now seldom used in the ocean.

The airfoil shear probe was originally devised by Siddon and Ribner (1965) for use in wind tunnel and atmospheric environments, and was modified for use in water by Siddon (1971). First tested in the ocean by T. Osborn in 1972 (Osborn 1974), it has since become the most effective tool for measuring oceanic velocity microstructure. Distinctly less problematic than its predecessor, the airfoil shear probe produces significantly larger signal outputs, and is completely insensitive to temperature fluctuations in the microstructure range. The primary disadvantage of using airfoil probes to measure velocity microstructure, however, is the tendency for probes to spatially average the smallest eddies of the turbulence (Fig. 1).

The finite size of the probe implies a lower limit on the eddy size that can be accurately measured. Since the shear spectrum shifts to smaller scales as dissipation rates increase, the error due to spatial averaging can be expected to increase with dissipation. This degree of attenuation of probe signal at high wavenumber remains a poorly understood phenomenon, despite past attempts by users of airfoil probes to correct for these effects. Oakey (1977) corrected his probe measurements using a single-pole model based on agreement with universal shapes, and Ninnis (1984) attempted to address the averaging issue by comparing a probe's response to a laser Doppler anemometer. The Ninnis response has been criticized for its prediction of a response null. This feature has never been observed, but the functional form of the response proposed by Ninnis was never intended to apply to wavenumbers near or beyond the ''predicted'' null.

The conventional airfoil shear probe, hereafter called the mantle after one of its principal components, has proved adequate for measurement of dissipation rates in the thermocline and at depth in the ocean. However, the measurement of higher dissipation rates in highly

Corresponding author address: Dr. Rolf Lueck, Ocean Turbulence Laboratory, Centre for Earth and Ocean Research, University of Victoria, L-Hut, Room 28, Victoria, BC V8W 3P6 Canada.
E-mail: rlueck@uvic.ca

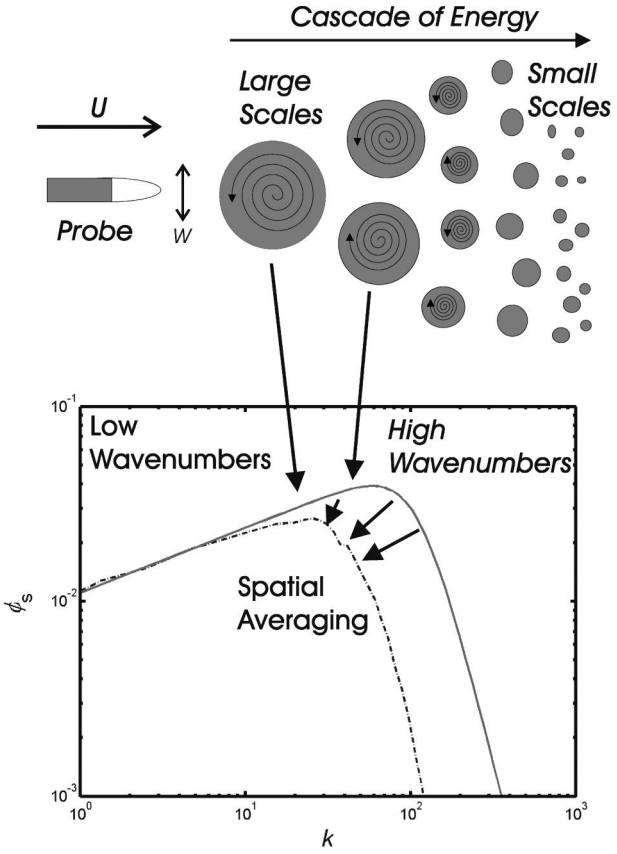

FIG. 1. The effect of spatial averaging on the shear spectrum of an airfoil probe. Here U denotes the mean travel speed and w the fluctuating cross-stream component of velocity. (solid line) The hypothetical true shear spectrum. (dashed line) The probe spectrum with spatial averaging.

turbulent areas, such as oceanic boundaries, is underestimated as a result of spatial averaging. This limitation due to probe size was the impetus for the development of a new, smaller airfoil probe, hereafter referred to as the bullet. The bullet has linear dimensions approximately one-half those of the mantle, and was expected to have twice the wavenumber resolution.

Without correction for the variance lost due to spatial averaging, shear spectra in elevated turbulence will undoubtedly yield dissipation estimates well below actual levels. For example, Rippeth et al. (2003) compared shear-probe-based dissipation estimates against the rate of production of turbulent kinetic energy derived from acoustic Doppler current profiler (ADCP) measurements in homogeneous turbulence and found that on average the dissipation rate was only 60% of the production rate, even though the two rates were expected to be equal. This discrepancy is within the range of variance lost due to spatial averaging by the shear probe for the rates of dissipation measured by Rippeth et al.

Our motivation is to estimate the wavenumber response of the airfoil shear probe, and to provide a means to correct probe signals for lost variance due to spatial averaging. Osborn and Crawford (1980) suggested that the spatial response of the probe may be revealed through the comparison of responses from a series of smaller probes. Comparing mantle and bullet responses to the same environmental signal provides a measure of the degree of spatial averaging by each probe. This insight, in conjunction with a one-dimensional model, illuminates the key dimension governing probe response and provides a means to correct each response for lost variance due to averaging.

The following section provides the theoretical background pertinent to this analysis, which includes a description of the turbulent shear spectrum, Nasmyth's universal form, the theoretical basis of the airfoil probe, and a summary of previous efforts to quantify spatial averaging. Section 3 provides a justification for the use of the single-pole filter as a model of spatial averaging, and explores the key dimensions of the probe. Section 4 outlines data specifics, the signal-processing techniques utilized to obtain average spectral estimates, and an optimization method used to determine the model parameters. Section 5 outlines the general results from this procedure, and sections 6 and 7 contain a discussion and conclusions.

2. Background

a. Kolmogorov hypothesis and the shear spectrum

In 1941, A. N. Kolmogorov published his seminal paper on the universal aspects of turbulence. His theory outlined the existence of a single spectrum describing turbulent motions, which arises from the nondimensionalization of wavenumber (k) by the ''Kolmogorov wavenumber'' (k_s), where

$$k_s = \frac{1}{2\pi}\left(\frac{\epsilon}{\nu^3}\right)^{1/4} \text{ (cpm)}. \quad (1)$$

Here, ϵ is the rate of dissipation of kinetic energy per unit mass, and ν is the kinematic viscosity of seawater. The only direct way to determine dissipation is to measure the variance of small-scale shear and/or the rate of strain. As ϵ increases, the variance of shear shifts to higher wavenumbers. When the wavenumber is normalized by k_s, the shear spectrum peaks at $0.125k_s$, and 90% of the variance resides at wavenumbers smaller than $0.513k_s$ (Wolk et al. 2002).

Shear spectra exhibit a $k^{1/3}$ power-law dependence between the largest scales (small k) where energy is injected, and the smallest scales (large k) where energy is dissipated through viscosity. For velocity spectra, the power law translates to a $k^{-5/3}$ dependence in this inertial subrange of wavenumbers, within which larger eddies merely transmit energy to smaller eddies. At wavenumbers beyond the inertial subrange, the shape of the shear spectrum and its eventual roll-off as k approaches k_s is not predicted by the Kolmogorov theory, and needs to be determined empirically (Nasmyth 1970), although

some essentially untested theories do exist (Panchev and Kesich 1969).

Eddies of comparable size to the probe are averaged, and the resultant recorded signals are strongly attenuated at these and smaller scales. Spatial averaging of the signal, especially at scales near the peak of the spectrum, can lead to serious underestimations of the variance, and hence the rate of energy dissipation. Kinematic viscosity ($\nu \approx 1.3 \times 10^{-6}$ m^2 s^{-1}) only varies by a factor of 2 in the world's oceans, but dissipation rates may vary by many factors of 10, and hence ϵ essentially determines the highest wavenumber that must be resolved.

b. The Nasmyth spectrum

Nasmyth (1970) used the same hot-film probes as Grant et al. (1962) and Gargett (1978) to measure longitudinal velocity fluctuations on the order of 1 mm (1000 Hz). He isolated three data segments taken from inshore waters where velocity fluctuations were large and temperature fluctuations were small. This 445 s of carefully chosen data provided a spectrum for velocity fluctuations now referred to as the Nasmyth spectrum. This spectrum is widely used to estimate variance not captured by the airfoil probe at higher wavenumbers and also serves as a general check on data quality. Assuming isotropy, the transverse (cross-stream) velocity spectrum (Φ_{22}), with respect to wavenumber, is given by

$$\Phi_{22}(k) = k_s^2(\epsilon\nu^5)^{1/4}F_2\left(\frac{k}{k_s}\right), \qquad (2)$$

where $k = \hat{k}(2\pi)^{-1}$ is the cyclic wavenumber (cpm), $\hat{k}$ is the radian wavenumber, and $F_2(k/k_s)$ is a nondimensional universal function that is predicted by Kolmogorov theory only in the inertial subrange. From (1) and (2), we see that the magnitude of the velocity spectrum is proportional to $\epsilon^{3/4}$, and that its bandwidth is proportional to $\epsilon^{1/4}$.

Nasmyth measured the longitudinal spectrum $\Phi_{11}(k)$ and derived $F_1(k/k_s)$. Oakey (1982) then derived $F_2(k/k_s)$ from $F_1(k/k_s)$ using the isotropic relationship

$$\Phi_{jj}(\hat{k}) = \frac{1}{2}\left[\Phi_{11}(\hat{k}) - \hat{k}\frac{\partial\Phi_{11}(\hat{k})}{\partial k}\right] \qquad (jj = 22, 33). \quad (3)$$

A deficiency in Nasmyth's predicted curve for the velocity spectrum is the limited quantity of rate of strain data used to establish this universal form. Although no range in dissipation rate is explicitly stated in his work, it seems likely that it was limited due to the short duration of measurement. There has been little attempt to use hot-film probes to establish the ''universal'' spectrum over a range of dissipation rates since Nasmyth's work, and hence his form still lacks confirmation over the many decades of dissipation that exist in the ocean.

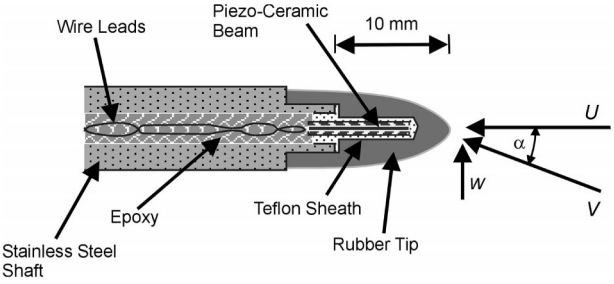

FIG. 2. A schematic diagram of the airfoil shear probe (courtesy of Fabian Wolk). The piezoceramic beam produces a charge proportional to the cross-stream lift force generated by flow around the probe.

c. The airfoil probe

For a detailed description of the airfoil probe designed for oceanic applications, refer to Osborn and Crawford (1980), Siddon and Ribner (1965), Siddon (1971), and Oakey (1977). The following is a brief outline of its principal components and theoretical framework.

The probe is a pointed body of revolution that utilizes hydrodynamic lift force to measure one cross-stream component of velocity. The cross-force on this axisymmetric surface is detected by an insulated strain transducer (Fig. 2). The transducer is a piezoceramic beam, which is composed of a material that generates a charge when subjected to a force or pressure. The construction of the piezobimorph beam is electrically equivalent to a parallel plate capacitor, where the electrodes are on each side and the piezoceramic is between the plates. The beam is attached to a charge sensitive amplifier with an integrating feedback capacitor C_f, and hence the voltage signal generated by a force is given by $V_{\text{out}} = Q/C_f$, where Q is the charge generated by the beam. The charge Q has some temperature dependence, whereas the charge sensitive amplifier C_f is generally stable with respect to temperature. The voltage output is passed through a differentiating circuit to improve the signal-to-noise ratio at higher frequencies and, in the presence of a constant speed through the water, becomes a measure of the along-stream gradient of cross-stream velocity fluctuations (Osborn and Crawford 1980). The probe is mounted so that its mean travel velocity through the water is aligned with the axis of revolution of the probe. This mean velocity is essentially the vehicle's rate of travel through the water, and the measured signal is the fluctuating flow orthogonal (or across-path) to this direction of travel.

The mantle's beam is secured inside a Teflon sleeve (mantle) with epoxy, which protects it from moisture. This sleeve is inserted into the end of a stainless steel shaft, and silicon rubber is molded over the tip to give the probe its characteristic shape (Fig. 3a). The bullet's transducer is inserted directly into a Teflon cap and is secured using epoxy. The outer surface of the cap is machined to the desired profile because the bullet is simply too small for the molding process (Fig. 3b). Due

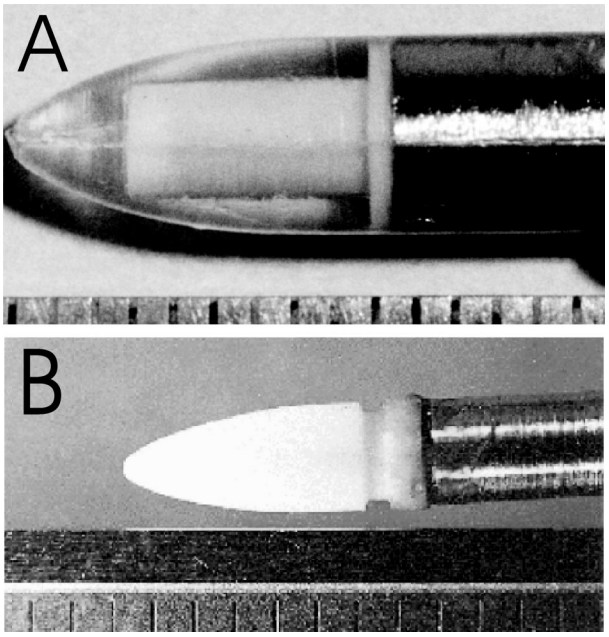

FIG. 3. (a) Mantle and (b) bullet airfoil shear probes. Scales are in mm. The bullet probe has linear dimensions roughly one-half those of the conventional mantle probe.

to its smaller size, and the much larger ($\approx 10\times$) thermal conductivity of Teflon compared to silicon, the bullet probe is sensitive to environmental temperature fluctuations below about 5 Hz ($\approx$5 cpm). Like Nasmyth, this forced us to be selective with our data.

For a slender body of revolution in an inviscid flow, the cross force per unit length due to the potential flow (Osborn and Crawford 1980) is given by

$$f_p = \frac{1}{2}\rho V^2 \frac{dA}{dx}\sin(2\alpha), \tag{4}$$

where ρ is the fluid density, A is the cross-sectional area of the probe, x is the distance from the tip along the probe axis, V is the instantaneous speed, and α is its angle of attack (Fig. 2).

The total cross force exerted on the probe is established by integrating (4) along the length of the probe from the tip (where $x = A = 0$) to the base (where $dA/dx = 0$ at $x = L$); that is,

$$F_p = \int_0^L f_p\, dx = \frac{1}{2}\rho V^2 A \sin(2\alpha)$$
$$= \rho A[V\sin(\alpha)][(V\cos(\alpha)] = \rho A U w, \tag{5}$$

where U is the velocity along the axis of the probe, and w is the fluctuating cross-stream component. One assumption in (5) is that the angle of attack is small, that is, $U \gg w$. The angle of attack must be smaller than $\approx 10^\circ$ for the shear probe to respond linearly to cross-stream velocity fluctuations (Osborn and Crawford 1980). The probes are calibrated in the range $\alpha = \pm 10^\circ$, and it is generally found that sensitivity can increase by up to 20% at $\alpha = 10^\circ$ compared to $\alpha = 0^\circ$. Maintaining a small α when the probe is mounted on a profiler is rarely a problem, however, because these instruments move through the water at speeds much greater ($\approx$1 m s^{-1}) than the magnitude of the cross-stream velocities (10–20 cm s^{-1}) (Lueck et al. 1997).

The output signal from an airfoil probe is thus described by

$$E_p = 2\sqrt{2}SUw, \tag{6}$$

where E_p is the probe voltage. The sensitivity S is determined by ρA and is proportional to the transformation of a mechanical force into a voltage by the ceramic strain sensor. The factor $2\sqrt{2}$ is an artifact of the method of calibration employed in our laboratory. Microstructure shear ($\partial w/\partial x$ and/or $\partial v/\partial x$) is obtained from the probe signal by applying the Taylor frozen field assumption

$$\frac{\partial}{\partial t} = U\frac{\partial}{\partial x}, \tag{7}$$

to the differentiated voltage E_p to give

$$E_s = \frac{\partial E_p}{\partial t} = 2\sqrt{2}SU^2\frac{\partial w}{\partial x}, \tag{8}$$

where E_s is the output from the analog differentiator. Under the assumption of local isotropy of the turbulence, the rate of dissipation of turbulent kinetic energy is determined using

$$\epsilon = 7.5\nu\overline{\left(\frac{\partial w}{\partial x}\right)^2} = 7.5\nu\overline{\left(\frac{E_s}{2\sqrt{2}SU^2}\right)^2}. \tag{9}$$

In practice, the variance of shear is obtained by integrating the shear spectrum in wavenumber space.

d. Correcting for spatial averaging

Some effort has been made over the last 30 yr to estimate and model the response of airfoil probes to determine the degree to which the probe signal is attenuated at high wavenumbers. Siddon (1971), by comparing the response of an airfoil probe (in air) to that of a set of crossed hot wires, found signal divergence occurring at wavelengths 4 times the diameter of the probe.

Oakey (1982) suggested that airfoil probes respond as single-pole low-pass filters, and estimated the effective wavelength of his probe to be $\lambda = 2 \pm 1$ cm. The form of his amplitude squared response estimate is

$$H^2(k) = \frac{1}{1 + \left(\frac{k}{k_c}\right)^2}, \tag{10}$$

where k is the cyclic wavenumber and k_c is the sensitive wavenumber ($k_c = \lambda_c^{-1} = 50$ cpm). Oakey's adoption of the single-pole transfer function was not justified on

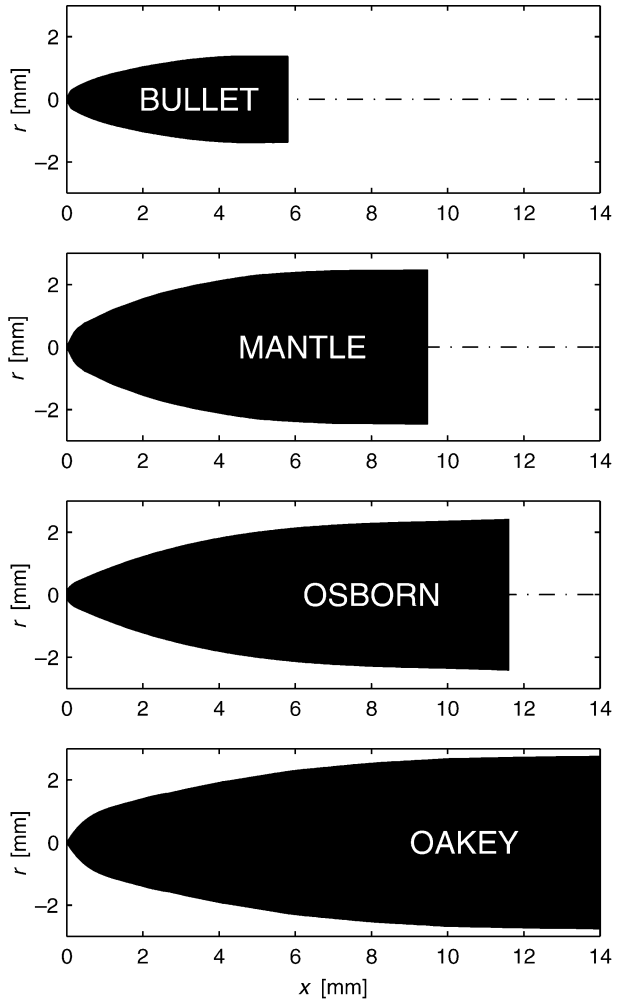

FIG. 4. Profiles of four different airfoil shear probes used to make dissipation estimates. Dynamic response estimates for the Osborn and Oakey probes were determined by Ninnis (1984). The bullet probe was first tested in Jun 1999.

theoretical grounds, but instead stemmed from agreement between corrected spectra and the Nasmyth spectrum at lower dissipation levels (Oakey and Elliot 1982).

In a coastal inlet, Gargett et al. (1984) simultaneously measured the streamwise component of velocity using the same heated platinum film probes as Grant et al. (1962), Nasmyth (1970), and Gargett (1978), and the cross-stream components of velocity using ''Osborn'' airfoil probes (Fig. 4). They established a version of the universal spectrum by applying a polynomial fit to their streamwise data (Φ_{11}), and, through isotropic relations, also established a universal transverse spectrum for comparison to Φ_{jj} measured by the airfoil probes (where $jj = 22, 33$). From the ratio of measured values from the probes, to the expected values for the transverse spectrum derived from Φ_{11}, they established a response for airfoil probes at high wavenumbers. The expression

$$R^2(k) = (1.033 - 8.836 \times 10^{-3}k + 3.379 \times 10^{-4})^{-1} \quad (11)$$

was used to correct all cross-stream spectra from airfoil probes. The above response function, when compared to (10), shows only marginally significant differences in the $20 < k < 40$ cpm range when $k_c = 65$ cpm. Also, Eq. (11) has a half-power point at 70 cpm.

Ninnis (1984) attempted to address spatial averaging by airfoil probes through the comparison of probe response to the output from a laser Doppler velocimeter in the far wake of laboratory grid turbulence. The test section of the water tunnel was a 30 cm $\times$ 30 cm cross section, that was 2 m long. The instruments were mounted 40 cm downstream from a biplanar grid with a mesh length of 1.27 cm and rod diameter of 0.32 cm. He observed that some low wavenumber downstream components had associated high wavenumbers in the cross-stream direction, suggesting the cross-stream averaging can remove some of the downstream energy. He developed a model that incorporated spatial averaging over the plane transverse to the direction of travel (due to the finite width of the probes), as well as averaging along the direction of the probe due to its finite length.

Ninnis' amplitude-squared response estimate for Oakey's probe (Oakey 1982) is given by

$$H^2(k) = \sum_{n=0}^{n=4} A_n \left(\frac{k}{k_0}\right)^n, \quad (12)$$

where $k_0 = 140$ cpm, $A_0 = 1$, $A_1 = -0.165$, $A_2 = -4.763$, $A_3 = 5.900$, and $A_4 = -1.986$. This response estimate is only meant to represent wavenumbers up to $\sim 0.7\ k_0$, where k_0 is the wavenumber of the first amplitude null. Ninnis also estimated the response of the Osborn probe (Osborn and Crawford 1980), which has a similar outside diameter to our conventional mantle probe (Fig. 4). Ninnis found half-power wavenumbers of 70 and 59 cpm for the Osborn and Oakey probes, respectively. For wavenumbers up to 80 cpm, Oakey's estimate ($\lambda = 2$ cm) and Ninnis' function are similar (Fig. 5). Beyond 80 cpm, the Ninnis response rolls off more steeply than (10), before rising again after $k = k_0$. It is important to recognize that the spectra of turbulence from laboratory grids are very different from oceanic spectra. There is little separation between energy-containing and dissipating scales, viscosity affects all wavenumbers, and there is very little (if any) inertial subrange. Extending laboratory measurements to oceanic turbulence, where there usually is an inertial subrange, must be done with caution and due reservation for the differences in turbulence characteristics.

3. The model

a. Justification for the single-pole model

We cannot begin to assess the degree of attenuation in a probe signal without first assuming an analytic form

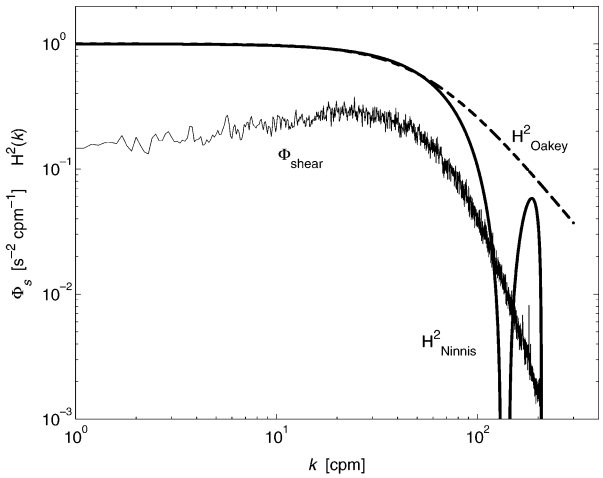

FIG. 5. Spectrum of the vertical shear from a mantle probe in a highly turbulent coastal channel compared with the dynamic transfer functions of Oakey (10) and Ninnis (12). The Ninnis response estimate is only meant to represent wavenumbers up to $\sim 0.7k_0$, where k_0 is the wavenumber of the first amplitude null.

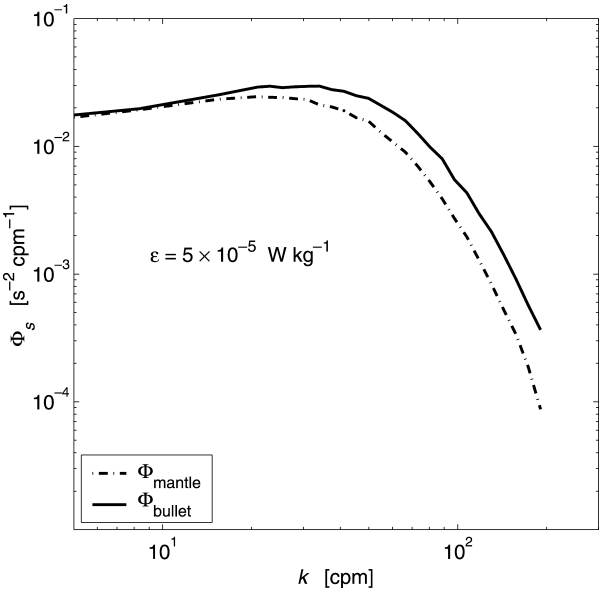

FIG. 6. Mantle and bullet probe spectra from file P_13. The probes were mounted side by side on TOMI's nose (3.3 cm apart). The ratio of these responses was the basis for the determination of the sensitive wavenumbers k_m and k_b.

to describe the physical process governing spatial averaging. Our choice is Oakey's transfer function [Eq. (10)], which assumes the response to be a linear function of a probe dimension. By comparing the response of different sizes of probe to the same environmental signal (Fig. 6), while assuming they both respond according to (10), we are provided with insight into their respective spatial resolutions and into the geometric connection to spatial averaging.

The Oakey response is a single-pole filter, and its only parameter is the single ''space constant''

$$l_c = \frac{\lambda_c}{2\pi} = \frac{1}{2\pi k_c}, \tag{13}$$

which is proportional to the inverse of the cut-off wavenumber (k_c), and is determined by some geometric dimension of the probe. The most attractive feature of this model is its simplicity. However, it is not obvious why a space constant should describe the probe response as opposed to some spatial filter like a top hat or an even more complicated spatial smoother. The space-domain weighting function that characterizes a single-pole filter is

$$h(x) = l_c^{-1} e^{-x/l_c}, \tag{14}$$

and this sort of response comes up naturally in simple systems with inertia. In this case, x might represent time instead of space, and l_c is the time constant. However, we know of no system or process that depends on a space constant. It is possible that the space constant proposed by Oakey is actually a time constant that appears as a space constant through the Taylor transformation of time into space.

The transverse force on the probe comes from the potential flow over the surface of the probe (Osborn and Crawford 1980), and this force is linear with respect to the angle of attack of the flow (for small angles of attack). Viscous stress is ignored in favor of the surface pressure distribution imposed by the inviscid potential flow. Let us assume that the angle of attack is initially steady and equal to zero. When an eddy approaches and then passes over the probe, the angle of attack will be disturbed. The streamlines around the probe, however, cannot change instantaneously, and it will take some time for the streamlines to adjust to the new angle of attack imposed by the eddy. The adjustment time will be comparable to the transit time of fluid passing over the probe. When this is viewed from a spatial perspective, the response is independent of flow speed and looks like an adjustment length that is comparable to the length (or some other relevant geometric feature) of the probe. That is, the probe must travel a distance l_c for the pressure distribution due to the potential flow to adjust to the new angle of attack imposed by the passing eddy.

The thin boundary layer over the surface of the probe is viscous, and the adjustment of flow within the boundary layer may take longer than the potential flow adjustment because of momentum diffusion. The time scale of diffusive adjustment is not inversely proportional to speed. If viscosity is important, then the probe space constant will not be independent of speed. The contribution of viscosity to probe response has not been specifically investigated. The calibrated sensitivities of our probes appear to be independent of speed over the range of 0.1–1.0 m s^{-1}, suggesting that viscosity is not important. In addition, the drag coefficients for cylinders

TABLE 1. The radial profiles of the mantle (r_m) and bullet (r_b) probes with respect to distance (χ) from the tip.

χ (mm)	r_m (mm)	r_b (mm)
0	0	0
0.12	0.28	0.28
0.41	0.70	0.48
0.70	0.89	0.62
1.00	1.06	0.74
1.29	1.22	0.84
1.58	1.35	0.92
1.87	1.48	1.00
2.17	1.60	1.07
2.46	1.70	1.13
2.75	1.79	1.18
3.05	1.88	1.23
3.34	1.96	1.28
3.63	2.03	1.31
3.93	2.09	1.34
4.22	2.15	1.36
4.51	2.21	1.37
4.80	2.26	1.37
5.10	2.30	1.37
5.39	2.33	1.37
5.68	2.36	1.37
5.93	2.38	—
6.41	2.41	—
6.89	2.43	—
7.37	2.44	—
7.85	2.44	—

and spheres are nearly independent of a Reynolds number for a Reynolds number of 5×10^3, which is the approximate value for a shear probe at our tow speeds.

Finally, it should be recognized that the response predicted by a single-pole filter and a spatial smoother, such as a top-hat function of length $(2.2 \times k_c)^{-1}$, are not very different for wavenumbers smaller than k_c. That is, it may be difficult to distinguish the single-pole model from other models when the signal attenuation is not large. However, a single-pole model provides a decidedly better fit to the shear probe data than does a double-pole model.

b. Probe geometry

The bullet is not an exact half-scale replica of the mantle probe. In order to establish ratios of the mantle's and bullet's linear probe dimensions, both probes were photographed and carefully measured (Fig. 3). The linear dimensions selected as influences on a probe's spatial resolution are diameter (near the fulcrum), length (from tip to fulcrum), and the distribution of dA/dx along the length of the probe.

The sensitive wavenumbers of the bullet and mantle probes are assumed to relate according to

$$k_b = R_s k_m, \tag{15}$$

where R_s is a length ratio based on relative probe dimensions. From Table 1, the ratio of mantle-to-bullet outside diameters indicates that $R_s = d_m/d_b = 1.78$. Siddon (1971) stated that the diameter is roughly equivalent to the relevant lift-producing dimension because of the characteristic shape of the airfoil probe (axisymmetric and low aspect ratio).

The mantle probe's piezoceramic beam is completely inserted and fixed into a Teflon sleeve. The outer profile of this sleeve increases in diameter abruptly at one end in order to securely fit into a stainless steel shaft (sting). The point at which the sleeve thickens to this diameter is the limit for beam sensitivity due to significantly enhanced stiffness. The significance of this length is somewhat ambiguous when considering the findings by Ninnis (1984) with regard to sensitivity along the axis of the probe. He found the Oakey and Osborn probes to have noticeably different sensitivity characteristics from tip to fulcrum. Also, both probes demonstrated a significant decrease in sensitivity well before the point of maximum bending. However, since we do not have further insight into the nature of the sensitivity for mantles and bullets along their axes, the fulcrum was selected as the limit for sensitivity and as a dimension for comparison. In the case of the bullet, there was concern that a Teflon cap would have excessive rigidity. In an attempt to enhance flexibility, a groove was machined into the fulcrum end of the Teflon cap (Fig. 3b). The midpoint of this groove is taken to be the point of maximum bending. The ratio of these sensitive lengths produces $R_s = 1.46$.

According to the theory outlined by (4), gain is proportional to dA/dx, and hence the sensitive part of the probe is determined by the distribution of cross-sectional area along the length of the probe. The radius measurements of both probes with respect to distance from their tips (x) were approximated using high-order polynomial fits. These fits were utilized to produce dA/dx curves (Fig. 7), and $(dA/dx)L$ curves, where L is the distance between the estimate for dA/dx and the fulcrum for each probe. This weighting of cross-sectional area is viewed as representative of the variation in sensitivity with distance away from the fulcrum, where probe sensitivity is high near the tip, and zero at the fulcrum. Below these curves, in Fig. 6, are their spectra normalized to unity at low wavenumber, which is a measure of how dA/dx and $(dA/dx)L$ influence spatial resolution for each probe. From these spectra we expect that $R_s = k_b/k_m = 1.53$ if dA/dx governs spatial resolution, and $R_s = k_b/k_m = 1.42$ if in fact dA/dx weighted by L is a better measure of probe sensitivity. If dA/dx or $(dA/dx)L$ is the only factor determining probe resolution, then the magnitude square of the Fourier transform of these spatial curves should give the wavenumber response of the probes (after normalizing to a response of 1 at a low wavenumber).

4. Analysis

a. Selection and processing of data

In June of 1999, mantle and bullet probes were used in side-by-side microstructure measurements in Sansum

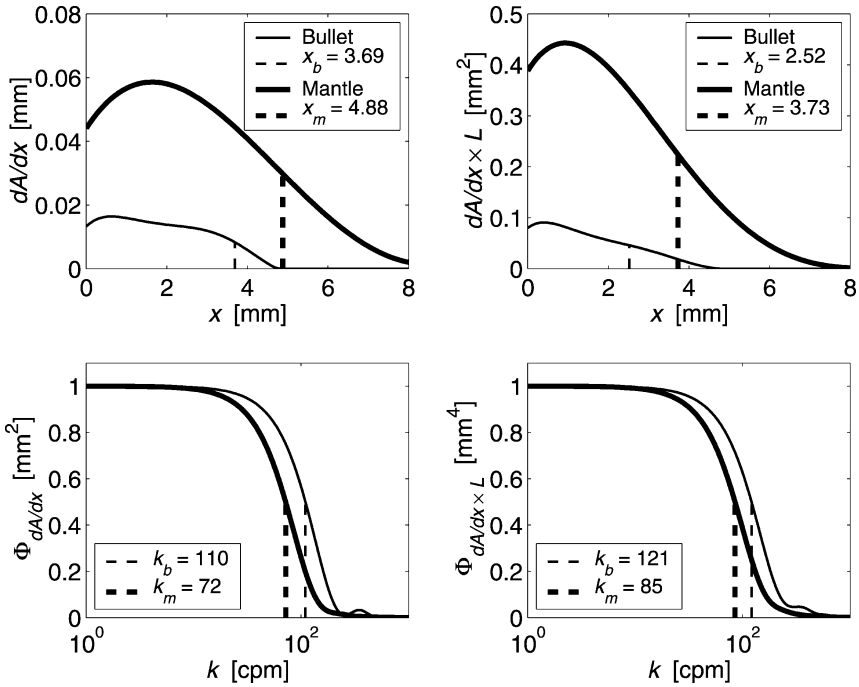

FIG. 7. (top left) Plot of dA/dx for bullet and mantle probes from polynomial fits to radius measurements. (top right) Plot of $(dA/dx)L$, where L is the distance between dA/dx and the fulcrum. Below each upper plot are the magnitude squares of the Fourier transform for each curve, which indicate half-power points of $k_m = 72$ cpm and $k_b = 110$ cpm for the dA/dx curves, and $k_m = 85$ cpm and $k_b = 121$ cpm for the $(dA/dx)L$ curves.

Narrows, British Columbia. From 5 days of tows using our horizontal profiler TOMI (Wolk and Lueck 2001), we collected over 34 h of turbulence data from which to draw for our comparison of respective probe responses at different dissipation rates. We towed TOMI for 6 days in August 2000, again in Sansum Narrows, and obtained additional data for comparison with the findings from 1999.

The data for this analysis were selected to encompass a range in dissipation rate and were screened for temperature contamination in the bullet probe. Three hours of shear data spanning $\epsilon = 5 \times 10^{-7}$ to 8×10^{-5} W kg^{-1} were ultimately selected and then divided into the 18 file segments summarized in Table 2.

Four different mantles and three bullets were employed at various times and in a variety of orientations

TABLE 2. A summary of the files used in the analysis and their corresponding optimum values for k_m and k_b.

No.	File	Length (s)	$\overline{U}$ (m s^{-1})	ϵ (W kg^{-1})	$\epsilon/\nu N^2$ (1×10^3)	k_m (cpm)	s	k_b (cpm)
1	P_01	560	1.10	5.0×10^{-5}	274	50.5	1.73	87.1
2	P_03	440	1.25	1.8×10^{-6}	9	60.5	1.90	114.6
3	P_05	250	1.19	4.3×10^{-5}	174	56.7	1.88	106.3
4	P_06	310	1.03	5.0×10^{-5}	432	46.9	1.80	84.2
5	P_08	400	1.32	5.0×10^{-7}	1	50.6	1.82	92.1
6	P_11	420	1.58	1.8×10^{-6}	5	45.4	1.82	82.6
7	P_12	500	1.54	9.0×10^{-6}	—	46.0	1.87	85.8
8	P_13	500	1.06	5.0×10^{-5}	—	49.4	1.81	89.2
9	P_14	500	1.38	8.0×10^{-5}	—	48.2	1.95	94.0
10	P_15	1880	1.43	2.5×10^{-6}	8	45.0	1.69	75.8
11	P_16	1880	1.25	4.0×10^{-5}	192	49.9	1.88	93.8
12	P_18	990	1.29	1.5×10^{-5}	31	48.7	1.75	85.2
13	P_20	470	1.09	8.5×10^{-6}	19	44.0	1.54	67.5
14	P_22	1000	1.76	5.0×10^{-5}	98	48.8	1.79	87.1
15	P_28	400	1.11	6.0×10^{-5}	115	48.2	1.67	80.3
16	P_29	400	0.95	5.0×10^{-5}	87	61.8	1.55	95.8
17	P_31	200	1.45	4.5×10^{-5}	22	53.3	1.78	94.9
18	P_33	500	1.01	2.8×10^{-5}	74	49.5	1.77	87.4

in these files. Our horizontal profiler supports up to four shear probes (3–5 cm apart, depending on position) at any given time, and probes can be oriented to sense either vertical or horizontal cross-stream velocity fluctuations. For highly turbulent files, a horizontal signal from a bullet probe can be compared to the vertical signal from a mantle probe, and vice versa. The assumption of isotropy was confirmed for these files by comparing spectra from the vertical and horizontal cross-stream components for like probes prior to comparing relative responses between mantles and bullets.

The probes were sampled at a rate of 512 samples per second and were low-pass filtered with a cutoff at 200 Hz. A typical vehicle speed of 1 m s^{-1} therefore provides us with a wavenumber bandwidth up to 200 cpm. Spectra for both types of probe were established using the periodogram technique, in conjunction with 50% overlap. Periodograms were calculated using consecutive 2-s intervals of shear data. Since shear spectra are a spatial, rather than temporal phenomenon, 2-s averages of velocity (U) were used to convert frequency (cps) to wavenumber (cpm). The final spectrum for each probe was compiled by ensemble averaging of the periodograms according to fixed wavenumber bins, which are uniformly distributed in logspace. The result of this technique is a smoother spectrum at higher wavenumbers (20–150 cpm) due to the wider bandwidth of high wavenumber bins. Further averaging of probe spectra was achieved by combining spectra from like probes.

A scaling adjustment to spectra was typically required at this stage in order to ensure different probe signals matched in the inertial subrange. Discrepancies in spectral level between mantle and bullet signals in the inertial subrange were common and have been attributed to temperature-related calibration errors. Large mean changes in temperature have an effect on the sensitivity [$S = S(T)$] of a probe and seem to affect mantle and bullet sensitivities differently. Our probes were calibrated in an average water temperature of 12°C. However, Sansum Narrows experiences temperatures ranging from 8° to 17°C, and hence probe sensitivities are not constant. To compensate for this effect, outlying spectra were scaled to match the ordinate level of the best apparent spectrum in the 5–15-cpm range. By scaling spectra we are in effect making minor adjustments to the sensitivity values for each probe, which results in spectral shifts parallel to the ordinate axis. The implied change in sensitivity to provide properly aligned spectra rarely exceeded ±5%, which is also the calibration error of S (±5%).

Below 5 cpm, bullet signals typically exhibited erroneous content due to low-frequency temperature fluctuations (see appendix). These spurious signals occasionally found their way to sufficiently high wavenumber to make the matching of spectra in the chosen range difficult. Mantle and bullet probes report different levels above 15–20 cpm in elevated turbulence due to spatial averaging, and hence 15 cpm was deemed a reasonable upper bound for alignment of spectra.

b. Parameter estimation

The single-pole, low-pass filter is a simple, one-dimensional model that describes spatial averaging through a single parameter, the sensitive wavenumber (k_c). For each file in Table 2, the sensitive or ''optimum'' wavenumbers for the mantle (k_m) and the bullet (k_b) were established by comparing the ratio of mantle spectra (Φ_m) and bullet spectra (Φ_b), to a single-pole response ratio defined by k_m and k_b.

The single-pole response ratio (mantle to bullet) is

$$R_H(k) = \frac{H_m^2(k)}{H_b^2(k)} = \frac{1 + \left(\frac{k}{k_b}\right)^2}{1 + \left(\frac{k}{k_m}\right)^2} = \frac{1 + \left(\frac{k}{s \times k_m}\right)^2}{1 + \left(\frac{k}{k_m}\right)^2}$$

$$(8 < k < 150 \text{ cpm}). \qquad (16)$$

We evaluated (16) over a large range of both k_m and s ($k_b = s \times k_m$) by establishing a 2D space over the ranges 30–70 cpm and 1 to 3 in steps of 0.1 and 0.01, respectively. The single-pole response ratio was computed for all possible combinations, giving 8×10^4 estimates of $R_H(k)$. The range for k_m was broader initially but was reduced after results indicated that k_m was well below the half-power wavenumber estimated by Ninnis (k_c = 70 cpm) for the Osborn probe. The range selected for s was chosen based on both Oakey's predictions and on the expected values for s previously discussed.

The optimum values of k_m and s for each file were determined by the estimate of $R_H(k)$ that provided the best fit to the measured spectral ratio $R_\Phi(k)$ [where $R_\Phi(k) = \Phi_m/\Phi_b$]. For each estimate of $R_H(k)$,

$$\overline{(|R_H(k) - R_\Phi(k)|)} \qquad (17)$$

was established over the wavenumber range $8 < k < 150$ cpm. The smallest value of (17) highlighted the best estimate of $R_H(k)$ from all possible estimates and yielded the optimum k_m and s values for that particular spectral ratio $R_\Phi(k)$.

A typical result from this optimization routine is shown in Fig. 8. The vertical scale on the right is the magnitude of the mean of the difference [Eq. (17)] between a ratio determined by (16) and a measured signal ratio (R_Φ). For the file represented in Fig. 8, the minimum value of (17) occurs at $k_m = 50.2$ and $s = 1.78$. The optimum k_m and s values for each file were calculated using this computationally efficient method and are tabulated in Table 2.

Figure 9 is a graph of R_Φ (○) for 500 s of shear data and its optimum response ratio R_H (solid line) determined from (17). Its associated optimum parameters are $k_m = 49.4$ and $s = 1.81$ ($k_b = 1.81 \times 49.4 = 89.4$

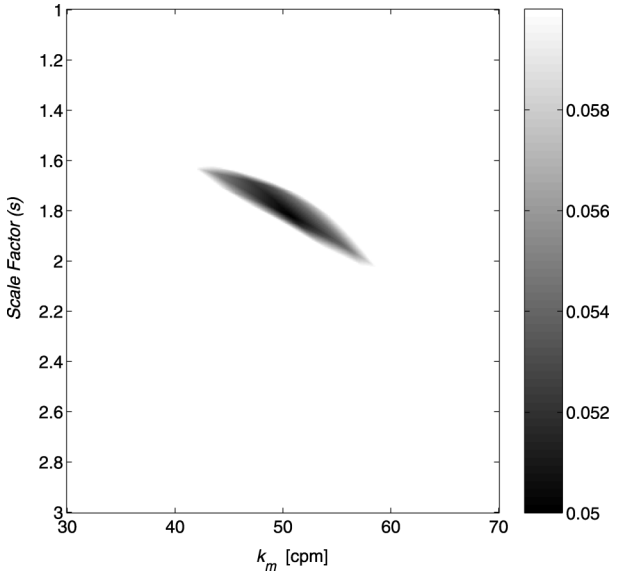

FIG. 8. Output from the optimization procedure. Optimal values for k_m and s listed in Table 2 are the combination of these two parameters that yield the minimum mean value of the difference between $R_H(k)$ and $R_\Phi(k)$ (gray shading scale). For this particular file, k_m = 50.2 cpm, s = 1.78, and k_b = 89.4.

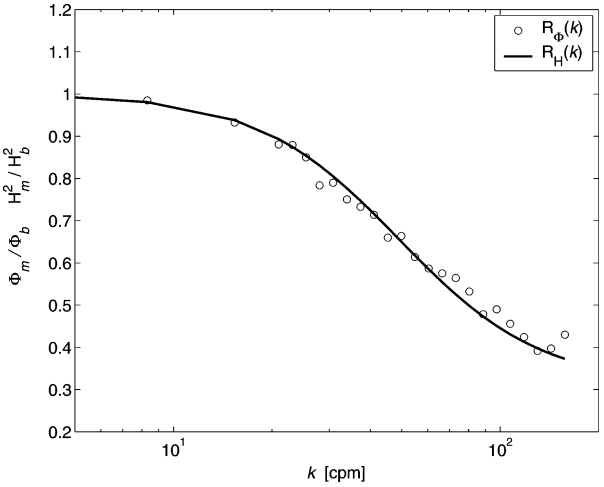

FIG. 9. The mantle-to-bullet spectral ratio $R_\Phi(k)$ (○) from file P_13 (see Fig. 7), and its optimum single-pole response ratio $R_H(k)$ (solid line), where k_m = 49.4 cpm and s = 1.81. Values below 5 cpm were not plotted on account of temperature contamination in the bullet signal. Here $R_H(k)$ coincides well with $R_\Phi(k)$ over all wavenumbers.

cpm). The improved resolution of the bullet probe over the mantle is evident through the dramatic drop in the signal ratio (vertical axis) at higher wavenumbers, and the use of a one-dimensional model to quantify this difference is clearly adequate.

5. Results

Table 2 summarizes the results of using a single-pole filter as a model for describing the spatial attenuation of signals generated by mantle and bullet shear probes. The optimum values for k_m range from 44 to 62 cpm (Fig. 10). Inspection of the results yields a grouping of k_m values in the limited range of 45–51 cpm. The median value is 49.1 cpm, and the mean is 50.2 cpm with a standard deviation of σ_k = 5.0.

The upper panel of Fig. 10 is a plot of k_m values with respect to dissipation level. It indicates the existence of a fixed value for k_m by virtue of the small range in k_m that was observed. This lack of systematic dependence of k_m on dissipation level further validates the hypothesis that response is simply a function of a linear dimension of the probe. For 3 h of turbulent shear data, ranging in dissipation rate from $\epsilon = 5 \times 10^{-7}$ to 8×10^{-5} W kg^{-1}, we find $k_m \approx 49$ cpm (k_m = 49.1 cpm is not only the median but also fits well over all dissipation levels).

Similarly, the scaling factor (s) that relates the bullet response to the mantle spans a range, from 1.55 to 1.95 (Fig. 10). As with k_m, the bulk of the estimates for s lie in a limited band. The median value is 1.80 and the mean is 1.78, with a standard deviation of σ_s = 0.11. We take s = 1.79, indicating k_b = 87.7 cpm (≈88 cpm). The dimension with a ratio closest to s = 1.79 is the diameter (R_s = 1.78). Based on this finding, the half-power wavenumbers for the Osborn and Oakey probes are k = 50 and k = 41 cpm, respectively.

Figure 11 is an assembly of all the spectral density ratios from measured signals used to establish k_m and k_b, along with the curve for $R_H(k)$ when k_m = 49 and k_b = 88 cpm. The curve produced by the single-pole model in Fig. 11 nicely overlays the measured ratios

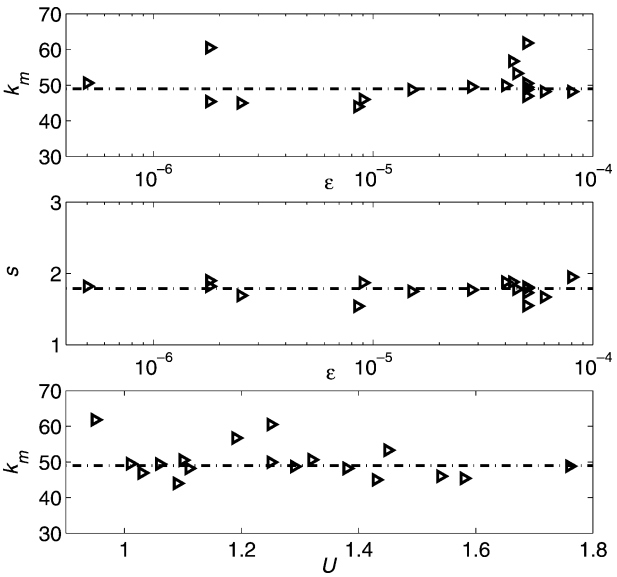

FIG. 10. The results of the optimization procedure [(top) k_m, (center) s] plotted with respect to dissipation rate. (dashed lines) The median values of k_m (49.1 cpm) and s (1.80). (bottom) Plot of optimum k_m values with respect to average velocity U. A lack of dependency of k_m on U suggests that molecular viscosity is unimportant for the adjustment process described in section 3a.

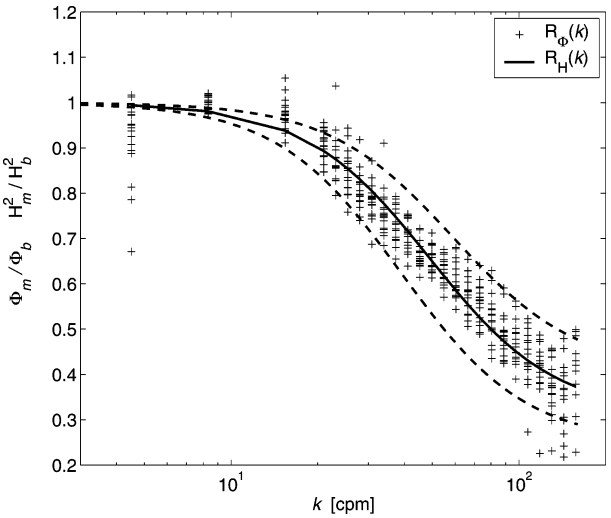

FIG. 11. Mantle-to-bullet spectral ratios $R_\Phi(k)$ (+) from all files, and the single-pole response ratio $R_H(k)$ (solid line) for $k_m = 49$ cpm and $s = 1.79$ ($k_b = 88$ cpm). Also plotted are confidence intervals (dashed lines) for $R_H(k)$ based on the standard deviations of k_m and s, where $k_m + 2\sigma k$ and $s - 2\sigma_s$ yield the upper bound and $k_m - 2\sigma_k$ and $s + 2\sigma_s$ provide the lower bound.

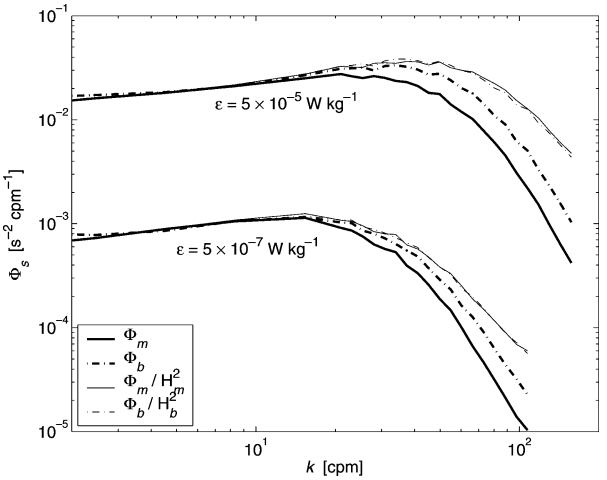

FIG. 12. Mantle (thick solid) and bullet (thick dashed) spectra for two dissipation rates and their corrected forms (thin solid and dashed).

and gives us confidence that our estimates for k_m and k_b are representative for all files.

When k_m and k_b are used to correct mantle and bullet signals, both signals take the same form and for the most part give identical measures of the dissipation rate (Fig. 12 and Fig. 13). In Fig. 13, the ordinate values from corrected mantle and bullet spectra are plotted against one another and coincide well over a range in dissipation rate. This agreement between corrected spectra from different probes further supports our estimate for s and allows us to compare corrected signals from either type of probe against the Nasmyth spectrum.

6. Discussion

a. Space constants

Through our comparative analysis of different sizes of airfoil shear probe, we have established half-power points of $k_m \approx 49$ cpm for the mantle probe and $k_b \approx 88$ cpm for the bullet probe. According to Eq. (13), these values correspond to space constants of $l_m \approx 3.2$ mm ($\lambda_m \approx 20.1$ mm) and $l_b \approx 1.8$ mm ($\lambda_b \approx 11.3$ mm). These values for λ_m and λ_b show a distinct similarity to the findings of Siddon (1971), who found signal divergence occurring at wavelengths 4 times the diameter of his probe. The diameter of the mantle and bullet probes are $d_m = 4.88$ mm and $d_b = 2.74$ mm, respectively, and 4 times these values are almost exactly equivalent to the half-power wavelengths λ_m and λ_b, where $4 \times d_m = 19.5$ mm and $4 \times d_b = 11.0$ mm. Although these similarities are encouraging, the complicated dependence of probe sensitivity on geometry remains somewhat unresolved at this time, due in part to the lack of observational support in this work for the expectation that dA/dx plays a role in probe sensitivity.

As previously discussed, l_m and l_b should not be speed dependent if molecular viscosity is unimportant for the adjustment process. From the lower panel in Fig. 10, we see that k_m shows no systematic dependence on the average speed through the water U, and hence we believe that viscosity plays a negligible role in the response of airfoil probes.

b. Corrected signals and Ninnis

In contrast to these findings, Ninnis' transfer function produced the half-power wavenumber $k = 70$ cpm for the Osborn probe, which has a similar diameter to the mantle probe. These findings suggest Ninnis' approach tends to underestimate the degree to which the environmental signal is attenuated. This implies that airfoil probe estimates of dissipation levels corrected using Ninnis' approach have in fact been too low and that, on average, dissipation levels are higher than previously thought. This observation, coupled with the inherent differences in wavenumber content between laboratory and oceanic flows, emphasizes the difficulties associated with comparing turbulent scales from these two environments.

c. Corrected signals and Nasmyth

Figure 14 shows the shear spectrum for a mantle, its corrected form, and the Nasmyth curve for a range in dissipation rate. The dissipation rates shown in Fig. 14 correspond to a fitted form of the Nasmyth curve that best fits the inertial subrange of the measured spectrum and is not the result of using the measured signal in conjunction with (9). This fitted form (Wolk et al. 2002) is described by

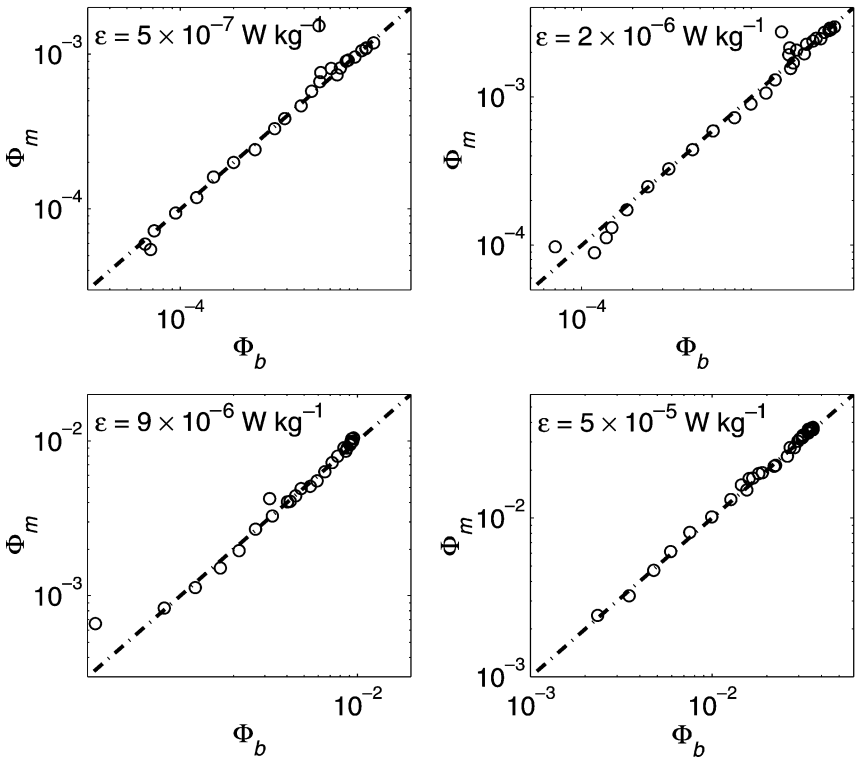

FIG. 13. Comparing ordinate values (○) from spectra of corrected mantle (Φ_m) and bullet (Φ_b) signals for different dissipation rates. (dashed line) An equivalent estimate from both. This comparison validates our estimate for s over a range in dissipation rate.

$$G_2(k_n) = \frac{8.05k_n^{1/3}}{1 + (20k_n)^{3.7}}, \tag{18}$$

where $k_n = k/k_s$ is the nondimensional wavenumber and $G_2(k_n)$ values correspond to those derived for the transverse spectrum by Oakey (1982) from Nasmyth's measurement of Φ_{11}.

At higher dissipation rates, a corrected mantle signal captures significantly greater variance than its original signal but is lower than what Nasmyth would predict. This variance discrepancy with respect to Nasmyth's spectrum is dependent on dissipation rate. From Fig. 14, corrected spectral estimates for both bullets and mantles are within 90% of the variance predicted by Nasmyth's estimate when $10^{-7} < \epsilon < 10^{-6}$ W kg^{-1}, which resembles Oakey's (Oakey and Elliot 1982) results when comparing corrected spectra using (10) to Nasmyth's estimate of the transverse spectrum. At dissipation levels higher than 10^{-6} W kg^{-1}, the corrected signals produce decreasing estimates of the shear variance relative to Nasmyth's curve, such that by $\epsilon = 10^{-4}$ W kg^{-1}, the corrected estimate is only 55% of the predicted variance.

This trend is summarized in Fig. 15, which shows the variance captured by the mantle probe, the bullet probe, and their corrected forms, relative to Nasmyth's estimate, for all data files. Dashed lines have been fit to the data points to highlight this increasing relative discrepancy with respect to dissipation rate. When considering intercepts, it appears that the corrected signals show equivalent variance to Nasmyth when $\epsilon < 2 \times 10^{-7}$ W kg^{-1}. In addition, the correction can be applied to signals below this dissipation rate without generating false variance since the effects of the single-pole model are much reduced at the lower wavenumbers characteristic of lower dissipation rates. For example, the mantle signal (thin solid line) in Fig. 14, which corresponds to $\epsilon = 5 \times 10^{-8}$ W kg^{-1} is little changed when corrected using the single-pole model (thick dashed line).

The discrepancy between Nasmyth's estimate and our corrected shear probe estimate brings various uncertainties in Nasmyth's work back to our discussion. How much faith can we have in a universal curve that represents all levels of dissipation, but is based on under 500 s of data at near constant dissipation rate? Furthermore, the transverse spectrum is a derivation based on his measurement of the longitudinal spectrum and the assumption of isotropy. To what extent should we be concerned about this derivation?

Further doubt in the universality of the velocity spectrum comes from work done by Doron et al. (2001), who used a particle image velocimetry (PIV) system to establish spatial energy and dissipation spectra for flows in the bottom boundary layer off the coast of New Jersey. PIV provides two-dimensional velocity distributions within a prescribed sample area that are true spatial

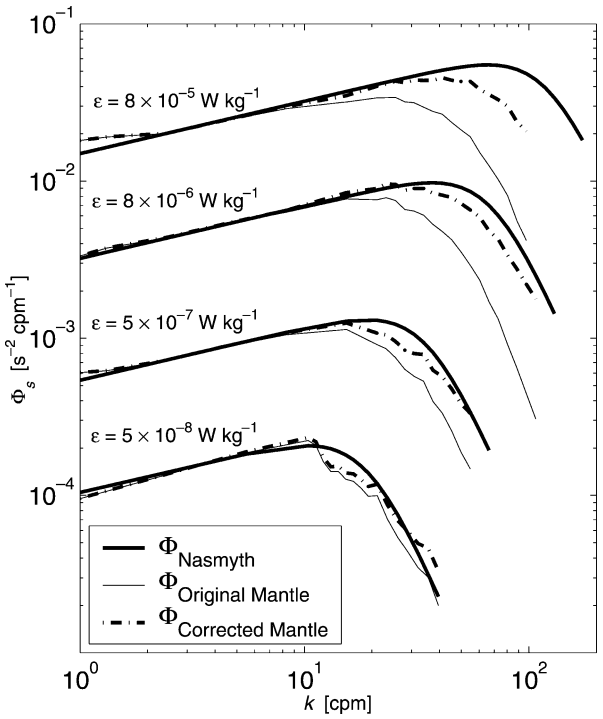

FIG. 14. Mantle spectra (thin line), their corrected form (thick dashed), and the Nasmyth curve (thick solid) for a range of dissipation rates. The corrected form of the bullet signal is adequately represented by the corrected mantle signal and is hence omitted for clarity. The corrected form of the mantle differs little from its original form at dissipation rates where spatial averaging is no longer an issue ($\epsilon \leq 10^{-8}$ W kg^{-1}).

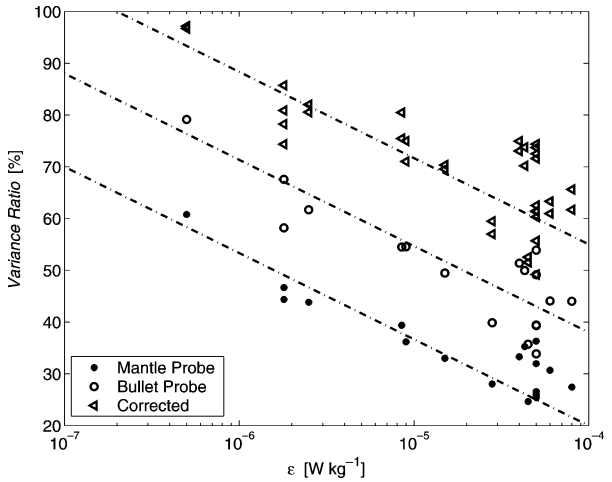

FIG. 15. The variance measured by the mantle, bullet, and their corrected form with respect to the Nasmyth estimate, for all files. (dashed lines) The decrease in the variance of all three signals relative to Nasmyth with increasing dissipation rate. The observed trend in the corrected spectra suggests that corrected signals capture all shear variance with respect to Nasmyth's predictions when $\epsilon < 2 \times 10^{-7}$ W kg^{-1}.

spectra since they do not involve the use of the Taylor hypothesis. Direct estimates of ϵ were established from the measured components of the deformation tensor, which were then compared to estimates from a number of methods based on assumptions of isotropy. The integrated Nasmyth universal curve, along with estimates from curve fitting in the inertial range and energy flux considerations, yielded 30%–100% higher rates of dissipation than the direct estimate. Furthermore, the data indicated a distinct lack of local isotropy at all scales, including the viscous dissipation range, as well as clear systematic differences between strain-rate spectra of velocity components parallel and perpendicular to the direction of the mean flow.

d. Isotropy

Gargett et al. (1984) (hereafter GON) carried out an in-depth analysis of spectral shapes from longitudinal and transverse shear measurements for the purpose of investigating the local isotropy of turbulence in a strongly stratified fluid. Their streamwise rate of strain measurements were made using a heated platinum film capable of resolving the entire dissipation spectrum (Φ_{11}), and the transverse shear estimates were made using airfoil probes. Their estimate of Φ_{11} showed small differences in high wavenumber shapes to Nasmyth's form and to the form predicted by Champagne (1978). They attributed these differences between all three estimates of the longitudinal velocity spectrum to errors in curve fitting to data points and recognized that these errors would propagate into the universal transverse form Φ_{jj} ($jj = 22, 33$). They found

$$\frac{\epsilon}{\nu N^2} \geq 200 \tag{19}$$

to represent the limit for the assumption of local isotropy at dissipative scales. This limit defines the conditions required for the employment of a single component of the velocity field to estimate dissipation rate. Values of (19) for the files employed in this analysis are well above this minimum requirement established by GON for the assumption of local isotropy (Table 2). Hence, our data appear to be from isotropic regions; however, the more recent findings of Doron et al. (2001) suggest that perhaps isotropy, even at dissipative scales, is not ensured.

7. Conclusions

A single-pole model for the wavenumber response of the airfoil probe closely predicts the relative response of our conventional probe (mantle) and a new half-size probe (bullet). Sensitive wavenumbers $k_m \approx 49$ cpm and $k_b \approx 88$ cpm were established by comparing the relative responses of mantle and bullet probes. The single-pole model indicates that the probe diameter near its fulcrum is the key geometric dimension influencing the wavenumber response. Ninnis' correction for spatial averaging of the probe signal suggests a larger value for k_m

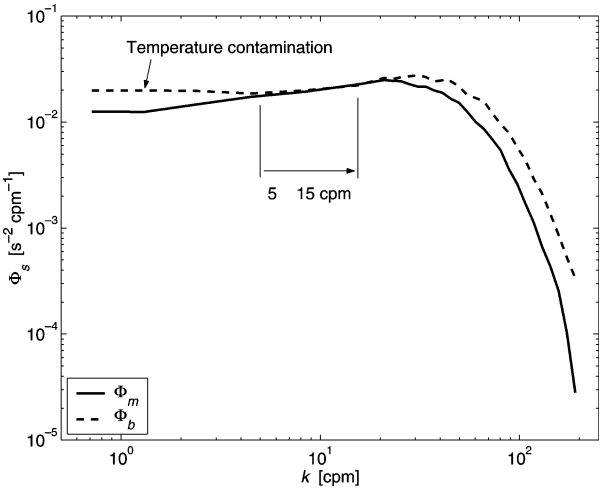

FIG. A1. Obvious contamination of the bullet spectrum at low wavenumber attributed to low-frequency temperature fluctuations. The bullet is more susceptible to thermal effects because its outer Teflon cap is more thermally conductive ($\approx 10\times$) than the silicon mold surrounding the mantle probe. Also shown is the wavenumber range (5–15 cpm) selected for the alignment of spectra in the inertial subrange.

than we have determined, and is viewed with skepticism due to the wavenumber differences between laboratory and oceanic flows.

Mantle (Φ_m) and bullet (Φ_b) shear spectra, when corrected using the single-pole model, agree well for dissipation rates in the range 5×10^{-8} to 8×10^{-5} W kg^{-1}. Corrected spectra at high wavenumber are systematically lower than the Nasmyth spectrum, and this discrepancy increases with increasing dissipation rate.

Acknowledgments. We thank the reviewers for their insight and comments, and Tom Osborn for useful suggestions. This work is supported by the U.S. Office of Naval Research under Grant N00014-93-1-0362.

APPENDIX

Signal Contamination

We encountered a significant degree of contamination at low wavenumbers in the bullet's signal as a whole. Low-pass filtered $\partial T/\partial x$ data from a thermistor and $\partial w/\partial x$ data from a bullet exhibit a clear correlation at low wavenumber, indicating the contamination is a result of low-frequency temperature fluctuations, which concurs with the prediction of Osborn and Crawford (1980).

The silicon mold protects the mantle's beam from temperature changes more effectively than the bullet's Teflon shell. The significant contamination of the bullet probe at a low wavenumber (Fig. A1) limits our ability to resolve large-scale features from its low-wavenumber content in thermally stratified turbulence. Until improvements to its thermal insulation are addressed, the bullet remains only useful for estimating dissipation levels from wavenumbers above 5 cpm.

REFERENCES

Champagne, F. H., 1978: The fine structure of the turbulent velocity field. *J. Fluid Mech.,* **86,** 67–108.

Doron, P., L. Bertuccioli, J. Katz, and T. R. Osborn, 2001: Turbulence characteristics and dissipation estimates in the coastal ocean bottom boundary layer from PIV data. *J. Phys. Oceanogr.,* **31,** 2108–2134.

Gargett, A. E., 1978: Microstructure and fine structure in an upper ocean frontal regime. *J. Geophys. Res.,* **83,** 5123–5134.

——, T. R. Osborn, and P. W. Nasmyth, 1984: Local isotropy and the decay of turbulence in a stratified fluid. *J. Fluid Mech.,* **144,** 231–280.

Grant, H. L., R. W. Stewart, and A. Moilliet, 1962: Turbulence spectra from a tidal channel. *J. Fluid Mech.,* **12,** 241–263.

Lueck, R. G., and T. R. Osborn, 1980: The characteristics of internally heated thermistors. *Deep-Sea Res.,* **27,** 273–292.

——, D. Huang, D. Newman, and J. Box, 1997: Turbulence measurements with a moored instrument. *J. Atmos. Oceanic Technol.,* **14,** 143–161.

Nasmyth, P. W., 1970: Oceanic turbulence. Ph.D. thesis, University of British Columbia, 69 pp.

Ninnis, R., 1984: The effects of spatial averaging on airfoil shear probe measurements of oceanic velocity microstructure. Ph.D. thesis, University of British Columbia, 109 pp.

Oakey, N. S., 1977: An instrument to measure oceanic turbulence and microstructure. Report Series BI-R-77-3, Bedford Institute of Oceanography, Dartmouth, NS, Canada, 52 pp.

——, 1982: Determination of the rate of dissipation of turbulent kinetic energy from simultaneous temperature and velocity shear microstructure measurements. *J. Phys. Oceanogr.,* **12,** 256–271.

——, and J. A. Elliot, 1982: Dissipation within the surface mixed layer. *J. Phys. Oceanogr.,* **12,** 171–185.

Osborn, T. R., 1974: Vertical profiling of velocity microstructure. *J. Phys. Oceanogr.,* **4,** 109–115.

——, and W. R. Crawford, 1980: *Air–Sea Interaction Instruments and Methods—An Airfoil Probe for Measuring Turbulent Velocity Fluctuations in Water.* Plenum Press, 801 pp.

Panchev, S., and D. Kesich, 1969: Energy spectrum of isotropic turbulence at large wavenumbers. *C. R. Acad. Bulgare Sci.,* **22,** 627–631.

Rippeth, T. P., J. H. Simpson, M. E. Inall, and E. Williams, 2003: Measurement of the rates of production and dissipation of turbulent kinetic energy in a tidal flow: Red Wharf Bay revisited. *J. Phys. Oceanogr.,* **33,** 1889–1901.

Siddon, T. E., 1971: A miniature turbulence gauge utilizing aerodynamic lift. *Rev. Sci. Instrum.,* **42,** 653–656.

——, and H. S. Ribner, 1965: An aerofoil probe for measuring the transverse component of turbulence. *Amer. Inst. Aeronaut. Astronaut.,* **3,** 747–749.

Wolk, F., and R. G. Lueck, 2001: Heat flux and mixing efficiency in the surface mixing layer. *J. Geophys. Res.,* **106,** 19 547–19 562.

——, H. Yamazaki, L. Seuront, and R. G. Lueck, 2002: A new profiler for measuring biophysical microstructure. *J. Atmos. Oceanic Technol.,* **19,** 780–793.